



OPEN

Dynamic characteristics of coal gangue subgrade filler under traffic load based on the hysteretic curves

Lian-Zhi Zhang¹, Cun-Bo Kang¹ & Zong-Tang Zhang²✉

Traffic cyclic loading is the key factor that leads to the deterioration of the long-term service behavior of subgrade. A series of cyclic triaxial tests was carried out by the large-scale dynamic and static triaxial apparatus (LSDSTA) to study the dynamic behaviors of coal gangue subgrade filler (CGSF) under multi-step cyclic loading using the morphological characteristics of hysteretic curves (MCHC). MCHC was quantitatively characterized by four parameters, i.e., the unclosed degree (ϵ_{ph}), inclination of long axis degree (k_{hl}), area (S_{hl}) and fullness degree (α_{hl}). With the increase of dynamic strain, ϵ_{ph} increases exponentially. k_{hl} of the coal gangue sample first decreases and then shows an increasing trend with the increasing dynamic strain. The values of S_{hl} are close to each other, and the energy dissipation in the sample is small. However, with the increase of dynamic strain, the specimen failure degree is increased, S_{hl} increases exponentially, and the damping ratio increases. With the increase of dynamic strain, α_{hl} increases approximately linearly. Confining pressure has a certain effect on the four parameters. These parameters can be recommended and used for quantitative analysis the dynamic behaviors of subgrade filler under traffic cyclic loading.

Keywords Subgrade, Dynamic triaxial, Coal gangue, Traffic loading, Hysteretic curve

In order to rationally utilize resources and save costs, nearby materials in the surrounding quarries should be used for subgrade filler in road engineering, while the construction of railways and highways has a huge demand for filling materials. Predatory mining in quarries has a significant impact on the surrounding environment and ecology. If coal gangue is used for the construction of subgrade, it will generate significant economic, social, and environmental benefits.

Coal gangue is a type of hard black rock with low carbon content, which is separated during mining and washing processes and becomes waste¹⁻³. The massive use of coal gangue waste has always been a hot topic concerned by many scholars⁴⁻⁷. The physical and chemical characteristics of coal gangue are similar to natural gravel, so coal gangue can be broken into coarse aggregate, which can decrease the exploitation of natural gravel, but also avoid a series of hazards caused by it⁸. Hence, the study on coal gangue aggregate has been focused by many scholars in recent years, such as⁹⁻¹². Comparatively, the demand of coal gangue as subgrade filler is greater, and the vast majority of existing coal gangue is suitable as a geotechnical filler¹³⁻¹⁵. Therefore, the effective utilization of coal gangue as subgrade filling has great practical significance.

Coal gangue used as subgrade filler is an important measure to solve the problem of coal gangue accumulation. In order to prevent the secondary environmental pollution caused by the coal gangue subgrade, a mature construction method, i.e., lay clay on the surface of the coal gangue subgrade, has been widely used^{16,17}. Then, coal gangue is widely used as subgrade filler with the rapid development of traffic construction in China. E.g., Jining-Yutai (Shandong-Jiangsu border) section of Ji Xu expressway, K127 + 760.000 section of Xu-Huai expressway¹⁸, Wangshan section of S102 in Anhui Province, Pinglin expressway, Qingxu section of 307 national highway, Xingtai-Hebei and Shanxi boundary of Xingfen expressway¹⁶. Therefore, the application of coal gangue as subgrade filler is feasible and extensive. The consumption of coal gangue used as subgrade filler is tremendous, which can effectively solve the problem of coal gangue accumulation.

There have been some researches on using coal gangue as subgrade filler materials. Jiao et al.¹⁹ the inorganic salt content and heavy metals of coal gangue used in Xing Fen expressway were analyzed through laboratory soak test and leaching test, groundwater in Xing Fen highway was captured, detected, evaluated and its quality

¹Geospatial Survey and Monitoring Institute of Hunan Province, Changsha 410000, People's Republic of China. ²Hunan Provincial Key Laboratory of Geotechnical Engineering for Stability Control and Health Monitoring, Hunan University of Science and Technology, Xiangtan 411201, People's Republic of China. ✉email: zzt@hnust.edu.cn

was good or excellent, and then coal gangue as a new filler can be applied to coastal highway roadbed. Li et al.²⁰ focused on the utilization of coal gangue aggregate in railway engineering for coal transportation passage. Chen et al.²¹ studied the effect of the compactive effort and initial particle gradations on the particle size distribution of mineral waste slag based on screening tests, and analyzed the effects of different factors such as the compactive effort, moisture content, coarse grain content (CGC, mass proportion of particles with sizes greater than 5 mm), and forming methods on the engineering properties of mineral waste slag to determine the reasonable roadbed construction parameters. Zhang et al.¹ investigated the permanent deformation and its unified model of coal gangue subgrade filler under traffic cyclic loading. Tang et al.²² studied the residual deformation of coal gangue subgrade filler under multi-vibration cyclic loading. In addition, the effect of gradation on the compaction and strength characteristics of coal gangue subgrade filler was also studied^{17,23,24}. As mentioned above, coal gangue is widely used as subgrade filler. The coal gangue subgrade is affected by the traffic dynamic loading in the actual environment, while there are few researches reporting the dynamic behaviors of coal gangue, especially considering coarse particles, used as subgrade filler under traffic cyclic loading.

Hysteresis curve morphological characteristics can characterize the important dynamic behaviors of the specimen, such as dynamic deformation, viscosity, stiffness, and energy loss. The study of dynamic characteristics of coal gangue subgrade filler based on the hysteretic curves is of great significance for understanding the dynamic behaviors of actual subgrade engineering under traffic load. Hence, a series of cyclic triaxial tests was carried out by the LSDSTA (large-scale dynamic and static triaxial apparatus) to research the dynamic properties of CGSF, i.e., coal gangue subgrade filler (the maximum particle size is 60 mm) under multi-step cyclic loading using the MCHC (morphological characteristics of hysteretic curves). MCHC was quantitatively characterized by four parameters, i.e., ε_{phl} , k_{hl} , S_{hl} , and α_{hl} , and then the residual strain, elastic properties, energy dissipation, and viscosity of CGSF under cyclic loading were analyzed to study the dynamic behaviors of CGSF.

Laboratory testing program

Tested materials and apparatus

The original tested materials of the specimens were crushed coal gangue, which were collected from a coal mine in Xiangtan city (as shown in Fig. 1). It should be noted that, the maximum particle size allowed by the test equipment in this test does not exceed 60 mm. Considering that the specimens in this test were prepared manually, CGSF with particle size greater than 60 mm were removed. Coal gangue particles are angular and sharp, rough surface, irregular shape and hard. The CGSF was dried to constant weight in an oven at 105 °C–110 °C (more than 24 h), and then the standard sieve tests with aperture sizes of 60, 40, 20, 10, 5, 2, 0.5 and 0.075 mm were carried out.

LSDSTA was used in this experiment, which is displayed in Fig. 2. In this apparatus, the mould is used to prepare the sample. Then the prepared sample is pushed into the triaxial pressure cover, and the testing machine control system that can automatically collect axial and volumetric deformation as well as pore pressure is used to achieve cyclic loading. The parameters of LSDSTA are displayed in Table 1. The sample size allowed by LSDSTA is $D = 300$ mm and $H = 600$ mm. The ratio between the triaxial specimen diameter and the maximum particle size should not be smaller than 5^{25–27}, therefore, the maximum particle size allowed by LSDSTA in this test does not greater than 60 mm, and then the effect of specimen size can be neglected. In addition, the large-scale triaxial tests and the same specimen size were widely used in the previous studies, e.g., Cai et al.²⁶ and Leng et al.²⁷, which guarantees there liability of this apparatus.

Experimental design

Considering that the fractal model gradation equation (FMGE) has a clear physical meaning and only one parameter facilitates the discussion of results. Therefore, the method of artificial preparation specimens is used according to FMGE in this test, and the FMGE is defined as^{28–31}



Figure 1. Coal gangue particles of each group after sieving tests.



Figure 2. The large-scale dynamic and static triaxial apparatus.

Parameters	Values
Specimen size (mm)	$\phi 300 \times 600$
Maximum axial static loading (kN)	≤ 1500
Maximum axial dynamic loading (kN)	≤ 700
Maximum axial displacement (mm)	≤ 90
Maximum confining pressure (MPa)	≤ 3
Maximum pore pressure (MPa)	≤ 3
Maximum vibration frequency (Hz)	≤ 5
Loading patterns	Half-sine wave, square wave, oblique wave, triangular wave, random wave and combined wave
Control system	Stress controlled loading, strain controlled loading and displacement controlled loading

Table 1. The parameters of LSDSTA.

$$P_i = \left(\frac{d_i}{d_{max}} \right)^{3-D_f} \times 100\% \quad (1)$$

where D_f represents the fractal dimension, d_i presents the particle size (mm), P_i denotes the cumulative mass percentage with particle size less than d_i (%), and d_{max} indicates the maximum particle size (mm).

The specimen gradation (i.e., particle size distribution) curve with $D_f = 2.37$ is shown in Fig. 3. The coefficient of uniformity (C_U) and the coefficient of curvature (C_C) are 17.19 and 1.90 respectively. Cylindrical specimen with $D = 300$ mm and $H = 600$ mm was utilized in this test, note that D and H are the diameter and height of the specimen, respectively. According to the Chinese Standard of Soils for Highway Engineering³², the maximum dry density (2.075 g/cm³) of the specimen is obtained.

Compaction degree, which was widely used for triaxial test and situ construction^{33,34}, is calculated as follows:

$$K = \frac{\rho}{\rho_{max}} \times 100 \quad (2)$$

where ρ_{max} denotes the maximum dry density (g/cm³), and ρ is the dry density of specimen (g/cm³), and K represents the compaction degree (%).

In this test, the compaction degree is used to control the preparation of specimens, and the compaction degree of specimen is 93%. In addition, the compaction degree meets the requirements of the road base and subbase materials.

Following the Chinese Standard of Soils for Highway Engineering³², to ensure the consistency of the specimen quality, a standard routine for the experimental procedure of the sample was used and the dry soil method was used to prepare samples. Figure 4 shows the process of the large triaxial tests, and the experimental steps are:

1. The drying CGSF should be well mixed according to the designed gradation curve (as shown in Fig. 3).
2. The specimen was compacted with a compaction hammer in a mould in five layers (as shown in Fig. 4b). Thickness of each individual layer was 120 mm, and the mass of added CGSF in each layer was near to 16 kg. Before placing CGSF for the next layer, the surface of the previously compacted layer was scraped to a depth of about 20 mm to guarantee well interlocking between the vertically adjacent layers. The target compaction

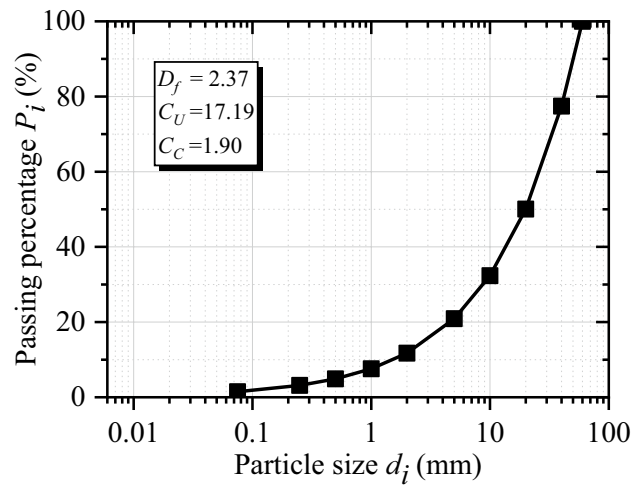


Figure 3. Particle size distribution of samples.

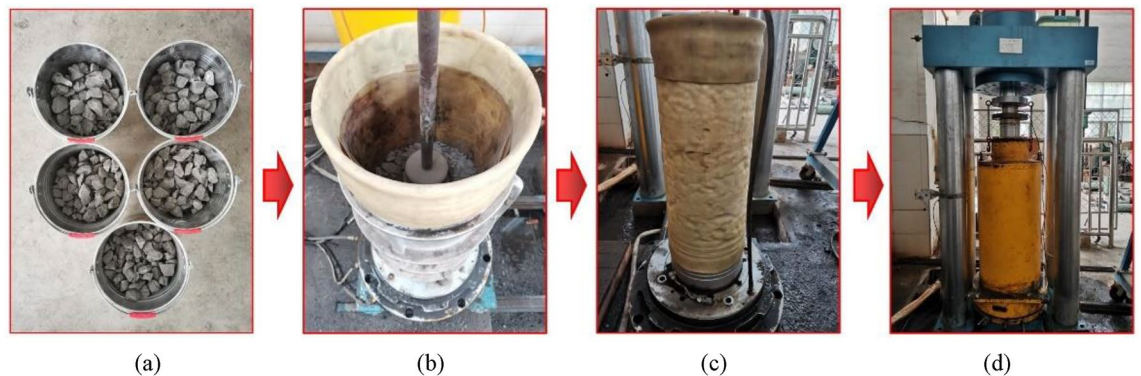


Figure 4. The process of the large triaxial tests: (a) CGSF required for a whole specimen; (b) compacting in a mould; (c) the prepared specimen; (d) enclosing the triaxial pressure cover.

- degree of the CGSF specimen was reached by controlling the thickness of each individual layer and the mass of added CGSF.
- After compaction, a rubber membrane was used to enclose the specimen, and the top and bottom of the specimen were tied with the rubber ropes. Figure 4c shows the prepared specimen.
- The specimen was put in the triaxial pressure cover, as shown in Fig. 4d. All of the specimens were saturated by back pressure before loading. The specimens were considered completely saturated when the pore pressure coefficient B was larger than 0.95.
- After that, the required effective confining pressure was applied to the specimen to complete the isotropic consolidation.
- Carry out cyclic triaxial tests using the large-scale dynamic and static triaxial apparatus.

The research shows that the traffic loading is different from the sine wave, but very similar to the half-sine wave³⁵. Therefore, the half-sine wave was used to simulate the traffic cyclic dynamic loading. The dynamic loading frequency was chosen as 1 Hz in these tests, which was also used in^{27,35}. This paper mainly focuses on the evolution of hysteretic curves of CGSF under different confining pressures, hence, the confining pressures (i.e., effective consolidation stress), σ_3' , of 50, 100, 150, and 200 kPa were selected in this test. Note that, three groups of parallel tests were carried out at the same time under each test condition, and first group was selected for key analysis. In order to ensure the uniformity of the specimen and eliminate the dispersion of the test results, step loading method was utilized in the dynamic triaxial test. Each step loading should be loaded 10 times, and the sixth complete loading process was mainly analyzed, which was also used in³⁶ and³⁷.

Cai et al.³⁸ defined cyclic stress ratio (CSR) as

$$CSR = \frac{\Delta q_{cyc}}{\sigma_3'} \quad (3)$$

The CSR was taken as 1, 1.5, 2, ..., until the specimen was destroyed, i.e., the test loading stopped when the accumulated strain reached 15%³⁶. The loading process in this test was shown in Fig. 5. According to Indraratna et al.³⁹ and Leng et al.²⁷, the relevant experimental parameters were defined as follows

$$q_{max,cyc} = \sigma'_{1max} - \sigma'_3 \quad (4)$$

$$q_{min,cyc} = \sigma'_{1min} - \sigma'_3 \quad (5)$$

$$\Delta q_{cyc} = q_{max,cyc} - q_{min,cyc} \quad (6)$$

$$\sigma_d = \Delta q_{cyc} / 2 \quad (7)$$

where σ'_1 represents the axial stress during cyclic loading (kPa); σ'_3 denotes the effective confining pressures (kPa); $q_{max,cyc}$ indicates the maximum cyclic deviatoric stress under different dynamic stress amplitudes (kPa); $q_{min,cyc}$ presents the minimum cyclic deviatoric stress under different dynamic stress amplitudes (kPa); σ_d denotes dynamic stress (kPa).

As mentioned above, CSR defined in Eq. (3) was used for stress controlled step loading test. Then, 10 numbers cyclic loading was used for each step loading, and the hysteresis loop under the 6th number cyclic loading of each step loading was selected for research. Hysteretic curve refers to the relationship curve between dynamic stress and dynamic strain with the coordinate origin as the center in one cyclic loading, and Fig. 6 displays the hysteresis curve of CGSF under different confining pressures. It can be seen from Fig. 6 that the hysteresis curve of CGSF under cyclic loading is approximately oval, and the hysteresis loop is not smooth. Furthermore, with the increase of dynamic strain and confining pressure, the gap between loading and unloading, the overall inclination angle, the enclosed area and the flattening degree of hysteresis curve have undergone great variation. Therefore, in order to accurately analyze the variation of hysteretic curve under cyclic loading, the unclosed degree (ε_{phl}), the inclination of long axis degree (k_{hl}), the area (S_{hl}) and the fullness degree (α_{hl}) for hysteretic curve were introduced to quantitatively investigate the evolution of MCHC of CGSF.

Quantitative analysis of MCHC

The hysteresis curve, also known as hysteresis loop, reflects the shape of dynamic stress- dynamic strain at different times in the process of unloading and reloading. Theoretically, the hysteresis curve is the curve of the forward helix along the transverse axis. In order to better study the periodic relationship between displacement and load, the center of each curve is translated to the coordinate origin. Further, the evolution of dynamic stress- dynamic strain can be fully understood by tracking the variation of hysteresis curve⁴⁰.

Hysteretic curve is the essential reflection of dynamic characteristics for materials under cyclic loading, and is the core for building the dynamic constitutive model of materials. MCHC can reflect the macroscopic mechanical characteristics of materials³⁷. Hence, the research on the MCHC has important theoretical and practical significance. Referring to the above studies, MCHC of CGSF under cyclic loading was made a quantitative analysis in this paper.

Analysis of the unclosed degree for hysteretic curve

Figure 6 illustrates the hysteresis curve of CGSF under different confining pressures. As observed in Fig. 6, the hysteresis curve of CGSF under cyclic loading is not closed. The starting point of hysteresis curve in Fig. 6 is at

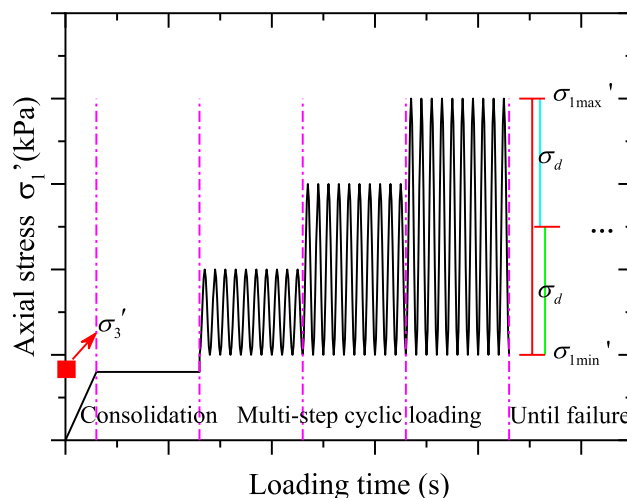


Figure 5. Loading process of specimen under cyclic loading.

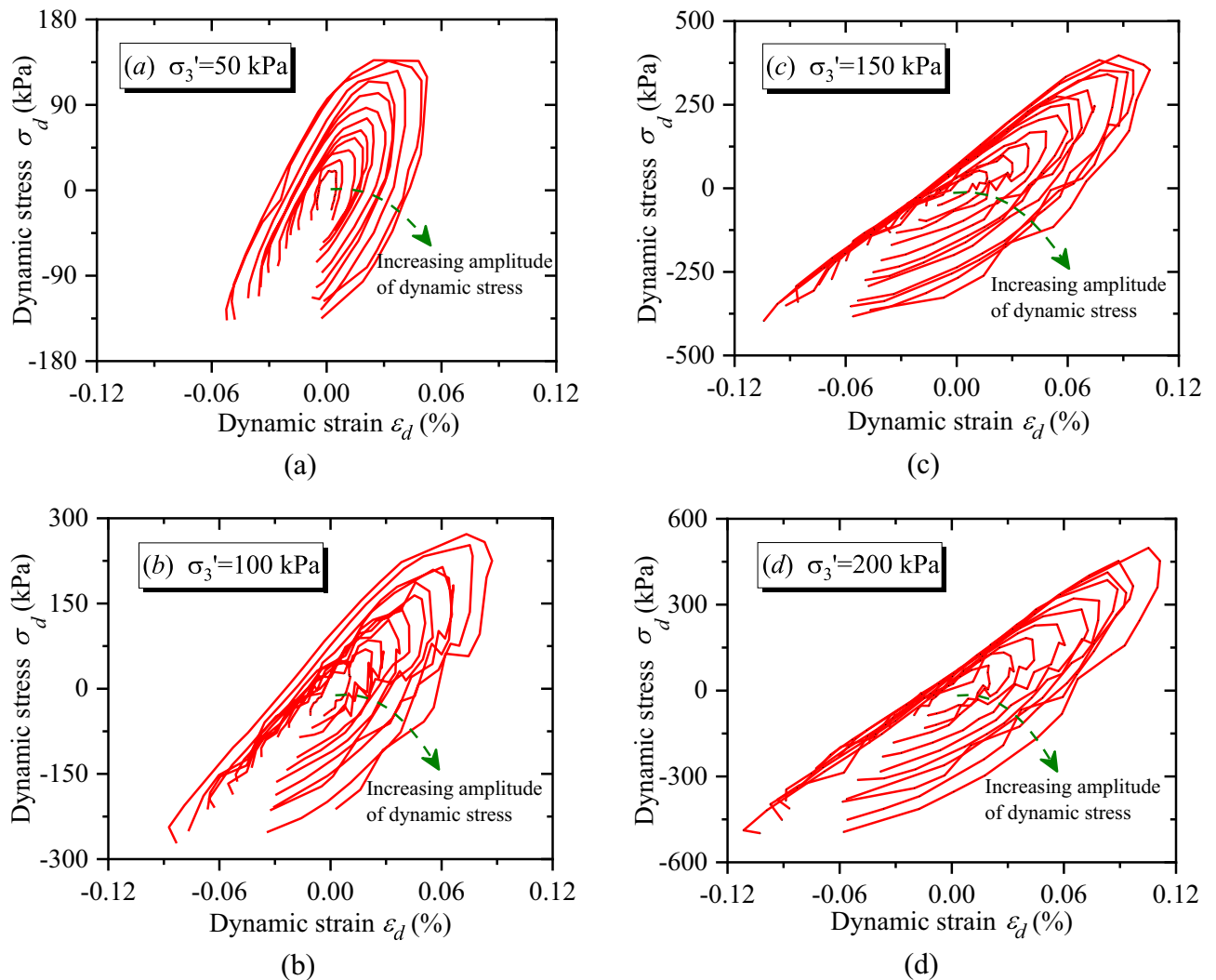


Figure 6. The hysteresis loops of CGSF: (a) $\sigma_3' = 50$ kPa, (b) $\sigma_3' = 100$ kPa, (c) $\sigma_3' = 150$ kPa, (d) $\sigma_3' = 200$ kPa.

the beginning of loading under cyclic loading in the test, and the end point of hysteresis curve is at the finish of unloading under cyclic loading. The difference between the strain corresponding to the loading beginning point (as shown in point A_l in Fig. 7) and the unloading finish point (as indicated in point B_l in Fig. 7) in one cycle is used to characterize the unclosed degree of the hysteresis curve (as demonstrated in Fig. 7, a schematic diagram for quantitative calculation of MCHC when the confining pressure was 50 kPa and the 60th step loading is taken as an example), which is defined as

$$\varepsilon_{phl} = |\varepsilon_{pe} - \varepsilon_{pb}| \quad (8)$$

where ε_{phl} indicates the unclosed degree of hysteresis curve, ε_{pe} denotes the unloading finish point (as indicated in point B_l) in one cyclic loading, and ε_{pb} represents the loading beginning point (as displayed in point A_l) in one cyclic loading.

The unclosed degree of hysteresis curve characterizes the residual strain after loading and unloading of one cyclic dynamic loading. As indicated in Fig. 6, the hysteresis curve of CGSF under cyclic loading is unclosed and asymmetric, which is due to the unrecoverable plastic deformation caused by cyclic loading for coal gangue sample. In addition, the center of hysteresis curve gradually moves towards the increasing direction of dynamic strain, which shows the behavior of gradually accumulated strain.

According to Eq. (8), the unclosed degree (ε_{phl}) of hysteresis curve can be captured. The relationship between ε_{phl} and dynamic strain (ε_d) is presented in Fig. 8. As demonstrated in Fig. 8, (1) With the increase of dynamic strain, the unclosed degree of hysteresis curve increases exponentially. It shows that the bigger residual deformation of CGSF occurs with the larger amplitude of dynamic stress. (2) As the increasing confining pressure, the unclosed degree of hysteresis curve decreases. The results show that the compaction effect of confining pressure on CGSF leads to the interlocking between coal gangue particle-particle enhancement, and the cohesion and friction force increase, which causes the residual deformation difficult to develop. Therefore, confining pressure

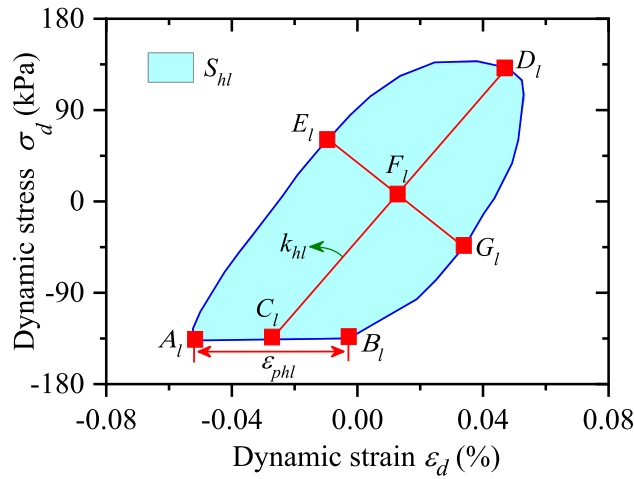


Figure 7. A schematic diagram for the calculation of MCHC.

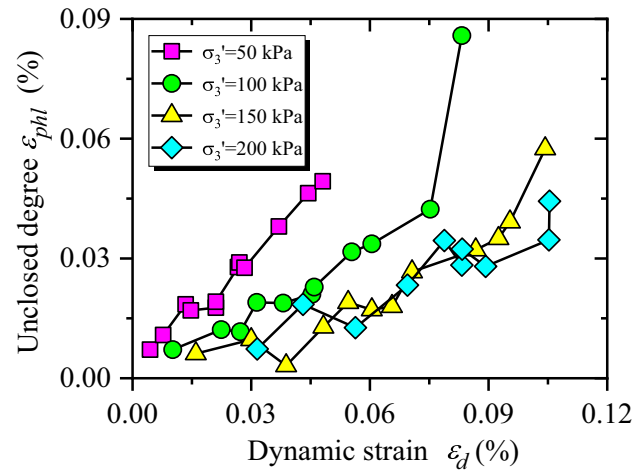


Figure 8. The relationship between ϵ_{phl} and ϵ_d .

has an obvious inhibitory effect on the development of unclosed degree. Zhuang et al.³⁷ studied the MCHC of improved expansive soil by using cylinder samples with a diameter of 50 mm and a height of 100 mm. However, due to the dynamic characteristic test including coal gangue coarse particles carried out in this test, the coarse particles will slip and break during the loading process, resulting in the hysteresis curve not smooth enough and some fluctuations in the curve.

Analysis of the inclination of long axis degree

As demonstrated in Fig. 6, the hysteresis curve of CGSF under cyclic loading is asymmetric in the process of loading and unloading, and the hysteresis curve is unclosed. The gradient of the straight line through two points, i.e., the turning point of the loading and unloading (such as point D_l in Fig. 7) and the midpoint of the starting and ending points of the loading and unloading (such as point C_l in Fig. 7) in one cyclic loading, is used to characterize the inclination of the long axis (k_{hl}) of the hysteresis curve. Then, the inclination of the long axis (k_{hl}) of the hysteresis curve is defined as

$$k_{hl} = \frac{\sigma_D - \sigma_C}{\epsilon_D - \epsilon_C} \tag{9}$$

where k_{hl} denotes the inclination of the long axis of the hysteresis curve, ϵ_D and σ_D represent the dynamic strain and dynamic stress at the turning point of loading and unloading in one cycle, respectively, ϵ_C and σ_C is the dynamic strain and dynamic stress at the midpoint of the starting and ending points of the loading and unloading in one cycle, respectively.

k_{hl} reflects the stiffness and elastic properties of CGSF. The greater k_{hl} has the better elastic properties of CGSF and the greater dynamic elastic modulus. On the contrary, the lower dynamic elastic modulus occurs with the smaller k_{hl} , and the specimen is easy to soften.

Relationships between k_{hl} and ε_d are displayed in Fig. 9. Obviously, k_{hl} of the coal gangue sample first decreases and then shows an increasing trend with the increasing dynamic strain. This shows that the resistance to deformation of the specimen is strong at the initial stage of step loading. Furthermore, with the increase of dynamic stress, the resistance to deformation of the specimen gradually decreases and slightly strengthened at the later stage of step loading. On the other hand, with the increase of confining pressure, k_{hl} of the hysteresis curve shows a gradually increasing trend, which means that the dynamic elastic modulus raises with the increasing confining pressure. With the increase of confining pressure, the initial stress of the coal gangue sample increases, the void ratio reduces, the cohesion and friction of the sample raise. Then the sliding between each particles becomes difficult, which improves the ability of specimen to resist deformation.

Analysis of the area for hysteretic curve

Because the hysteresis curve is unclosed, the starting and ending points of the loading and unloading in one cycle is connected in this paper, and then the area of the closed hysteresis curve is solved. Firstly, the hysteresis curve is artificially divided into two sections, i.e., the gradient is positive or negative. Then the area enclosed by the hysteresis curve with negative gradient and the abscissa axis is subtracted from the area enclosed by the hysteresis curve with positive gradient and the abscissa axis to calculate the area of the hysteresis curve, and the calculation formula is

$$S_{hl} = \frac{1}{2} \sum_{i=1}^n (\sigma_i + \sigma_{i+1})(\varepsilon_{i+1} - \varepsilon_i) - \frac{1}{2} \sum_{j=1}^m (\sigma_j + \sigma_{j+1})(\varepsilon_{j+1} - \varepsilon_j) \quad (10)$$

where S_{hl} presents the area of the hysteresis curve; ε_i and σ_i are the dynamic strain and dynamic stress at each point in the hysteresis curve with positive gradient, respectively; ε_i and σ_i indicate the dynamic strain and dynamic stress at each point in the hysteresis curve with negative gradient, separately.

The area of hysteresis curve reflects the energy dissipation of coal gangue sample due to damping. The larger area of the hysteresis curve has the greater energy dissipation of the sample under one cyclic loading.

S_{hl} of CGSF can be obtained by Eq. (10), and the evolution of S_{hl} versus ε_d is illustrated in Fig. 10. As shown in Fig. 10, the curves are intertwined and difficult to distinguish under the condition of small strain. Therefore, the embedded diagram is displayed in Fig. 10 to show the curve variation with dynamic strain (ε_d) less than 0.04%. It can be seen from Fig. 10 that the sample can rebound sufficiently when the dynamic strain is small ($\varepsilon_d < 0.04\%$). Hence, the values of S_{hl} are close to each other, and the energy dissipation in the sample is small. However, with the increase of dynamic strain, the sample is gradually compressed. Then, the specimen failure degree is increased, S_{hl} increases exponentially, and the damping ratio increases. With the increasing confining pressure, S_{hl} shows a decreasing trend.

Analysis of the fullness degree

As observed in Fig. 6, the fullness degree of hysteresis curve is various under different test conditions. Hence, α_{hl} is used to analyze the fullness degree of hysteresis curve, which is defined as

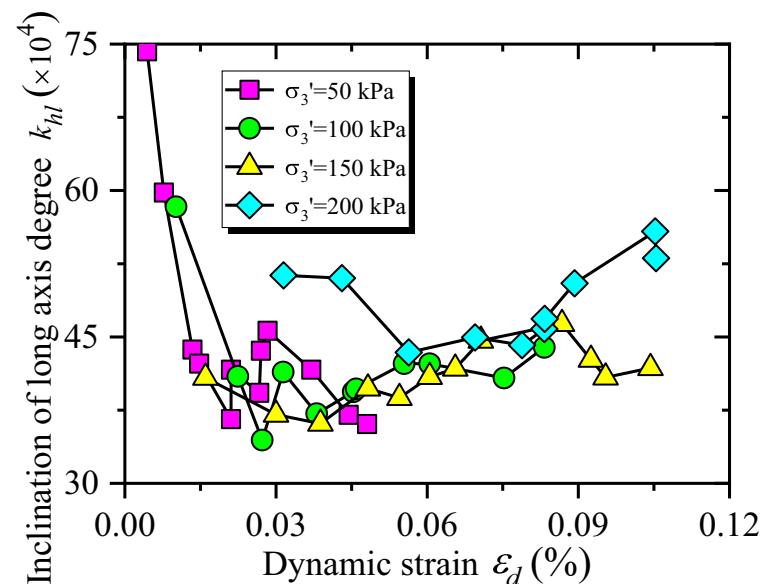


Figure 9. The relationship between k_{hl} and ε_d .

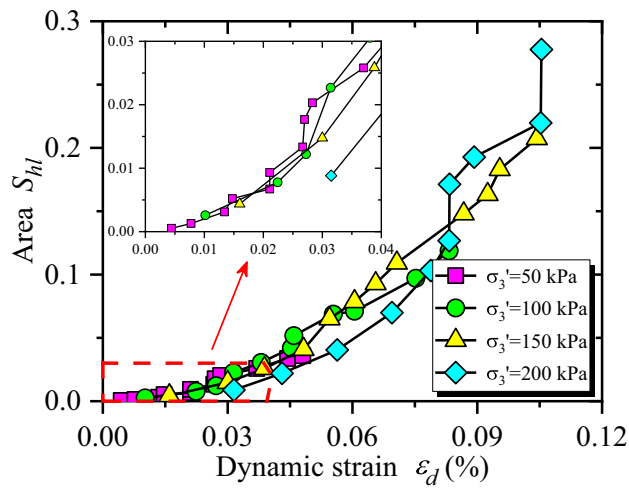


Figure 10. The relationship between S_{hl} and ε_d .

$$\alpha_{hl} = \frac{b_{hl}}{a_{hl}} \tag{11}$$

where α_{hl} presents the fullness degree; b_{hl} is the length of the long axis for the hysteresis curve, i.e., the distance between point C_l and point D_l in Fig. 7; a_{hl} represents the length of the short axis for the hysteresis curve, considering that the loading and unloading of the hysteresis curve as shown in Fig. 6 is asymmetric and not smooth, the sum of the line segment E_lF_l and F_lG_l is taken as a_{hl} , i.e., the sum of the maximum distance between the loading and unloading section of the hysteresis curve and the straight line C_lD_l .

α_{hl} reflects the viscosity of CGSF, the greater α_{hl} has the bigger viscosity. In the hysteresis curve of CGSF shown in Fig. 6, the thinner hysteresis curve occurs with the smaller α_{hl} , and the fatter hysteresis curve indicates the larger α_{hl} .

Relationships among α_{hl} and ε_d are illustrated in Fig. 11, with the increase of dynamic strain, α_{hl} increases approximately linear, and the influence of confining pressure on α_{hl} is significant, that is, the greater the confining pressure is, the smaller the α_{hl} will be. Further, with the increasing dynamic strain, particles of CGSF are gradually compacted, and then particle sliding or even breakage occurs. The structure of the sample is failed, and the unrecoverable plastic deformation is gradually generated. Under cyclic loading, the viscosity of the sample increases, and the hysteresis curve becomes fuller. The larger confining pressure results in the closer contact between particle and particle, the more compact sample, the lower viscosity of sample under cyclic loading, and the thinner hysteresis curve. In this test, under the condition of small strain, the coarse particles of the sample were gradually compacted, and the elastic energy was not obvious enough, so there was no obvious turning point in the test results.

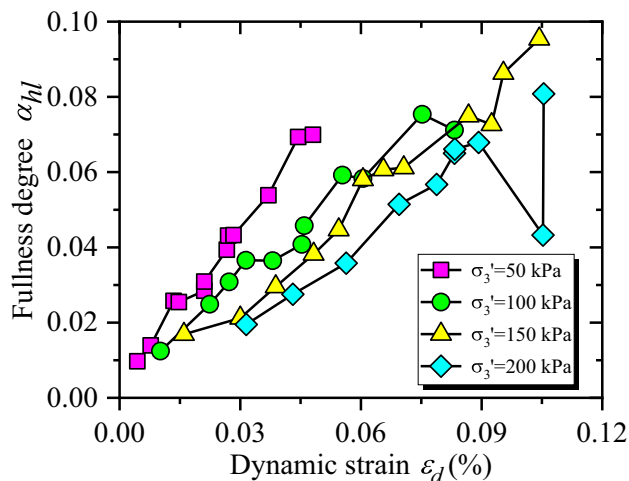


Figure 11. The relationship between α_{hl} and ε_d .

Conclusions

Hysteresis curve morphological characteristics can characterize the important dynamic behaviors of the specimen, such as dynamic deformation, viscosity, stiffness, energy loss, dynamic modulus, damping ratio. Therefore, the study of dynamic characteristics of coal gangue subgrade filler using the hysteretic curves is of great significance for understanding the dynamic behaviors of actual subgrade engineering under traffic load. Based on the large-scale dynamic triaxial tests of coal gangue subgrade filler, the following conclusions can be drawn from the above investigation.

1. The hysteresis loop of CGSF under cyclic loading is approximately oval and not smooth. The detailed calculation method of MCHC parameters was proposed, and then the MCHC parameters were used to quantitatively investigate the evolution of MCHC of CGSF.
2. With the increase of dynamic strain, ε_{phl} increases exponentially. Confining pressure has an obvious inhibitory effect on the development of ε_{phl} , as the increasing confining pressure, ε_{phl} decreases.
3. k_{hl} of the coal gangue sample first decreases and then shows an increasing trend with the increasing dynamic strain. Furthermore, with the increase of dynamic stress, the resistance to deformation of the specimen gradually decreases and slightly strengthened at the later stage of step loading. On the other hand, with the increase of confining pressure, k_{hl} shows a gradually increasing trend, which means that the dynamic elastic modulus raises with the increasing confining pressure.
4. The values of S_{hl} are close to each other, and the energy dissipation in the sample is small. However, with the increase of dynamic strain, the specimen failure degree is increased, S_{hl} increases exponentially, and the damping ratio increases. With the increasing confining pressure, S_{hl} shows a decreasing trend.
5. With the increase of dynamic strain, α_{hl} increases approximately linearly, and the influence of confining pressure on α_{hl} is significant, that is, the greater the confining pressure is, the smaller the α_{hl} will be.

Data availability

The datasets used and/or analysed during the current study available from the corresponding author on reasonable request.

Received: 7 September 2023; Accepted: 16 May 2024

Published online: 21 May 2024

References

1. Zhang, Z.-T., Wang, Y.-H., Gao, W.-H., Hu, W. & Liu, S.-K. Permanent deformation and its unified model of coal gangue subgrade filler under traffic cyclic loading. *Appl. Sci.* **18**, 2865 (2023).
2. Yang, Z. Y. *et al.* Medium-temperature calcination and acid pressure leaching extract the Al₂O₃ from coal gangue: Activation mechanism and kinetic analysis. *RSC Adv.* **14**, 11266–11275 (2024).
3. Wang, Z. G., Ma, H. Q. & Niu, X. Y. Study of mechanics and durability of non-spontaneous combustion coal gangue coarse-aggregate high-performance concrete. *Materials* **2024**, 17 (2024).
4. Wang, H. C. *et al.* Insight into the fracture mechanical properties of the interfacial transition zone of cemented coal gangue backfill under different stress angles by mesoscopic digital image correlation. *Eng. Fract. Mech.* **2024**, 300 (2024).
5. Li, Y. X. *et al.* Effect of activated coal gangue on the hydration and hardening of Portland cement. *Constr. Build. Mater.* **2024**, 422 (2024).
6. Guan, X., Ji, H. Y., Qiu, J. S. & Xiao, Q. H. Effect of freeze-thaw damage and pore structure on capillary water absorption of gangue-based concrete. *Ksce J. Civ. Eng.* **28**, 2315 (2024).
7. Wang, J. L., Duan, Y. X., Lyu, X., Yu, Y. & Xiao, J. X. Axial compression behavior of coal gangue coarse aggregate-filled steel tube stub columns. *J. Constr. Steel Res.* **2024**, 215 (2024).
8. Xiao, G., Yang, G., Jixi, C. & Ruyi, Z. Deterioration mechanism of coal gangue concrete under the coupling action of bending load and freeze–thaw. *Constr. Build. Mater.* **338**, 127265 (2022).
9. Li, Y., Liu, S. & Guan, X. Multitechnique investigation of concrete with coal gangue. *Constr. Build. Mater.* **301**, 124114 (2021).
10. Qiu, J., Zhu, M., Zhou, Y. & Guan, X. Effect and mechanism of coal gangue concrete modification by fly ash. *Constr. Build. Mater.* **294**, 123563 (2021).
11. Zhao, B. *et al.* Rheological properties, mechanical characteristics, and microstructures of gangue-cemented paste backfill: Linking to loess doses. *Arab. J. Geosci.* **15**, 244 (2022).
12. Zhao, Y. *et al.* Toward understanding the activation and hydration mechanisms of composite activated coal gangue geopolymer. *Constr. Build. Mater.* **318**, 125999 (2022).
13. Shen, W. S., Zhao, P., Wang, X. C. & Wang, J. C. Study the performance of coal gangue filling in the road embankment. In *International Conference on Civil, Architectural and Hydraulic Engineering (ICCAHE 2012) 1953–1956* (2012).
14. Song, G. Y. *et al.* Analysis of pH and conductivity variation characteristics of coal gangue used in freeway subgrade and its correlation. In *Asia Conference on Geological Research and Environmental Technology (GRET) Electr Network* (2020).
15. Hui, B. *et al.* Study on stress characteristics of high-porosity coal gangue subgrade during filling process. *J. Theor. Appl. Mech.* **61**, 625–641 (2023).
16. Zhou, N. *et al.* Present situation and prospect of coal gangue treatment technology. *J. Min. Saf. Eng.* **37**, 136–146 (2020) ((in Chinese)).
17. Zhang, Z. Dynamic behaviors and the evolution of particle breakage for coal gangue subgrade filler under cyclic loading. In *Xiangtan: Hunan University of Science and Technology* (2021).
18. Sun, K., Peng, F., Yang, G., Ge, Y. & Song, Z. Disease research and construction technology of Xupu-Huaihua high-speed gangue embankment culvert. *Constr. Technol.* **47**, 1170–1173 (2018) ((in Chinese)).
19. Jiao, S. J., Wang, S. & Luo, F. Z. Effects of coastal coal gangue highway on groundwater. In *2nd Global Conference on Civil, Structural and Environmental Engineering (GCCSEE 2013) Shenzhen 2518* (2013).
20. Li, L. H. *et al.* Utilization of coal gangue aggregate for railway roadbed construction in practice. *Sustainability* **2020**, 12 (2020).
21. Chen, M., Wen, P., Wang, C., Chai, Z. & Gao, Z. Evaluation of particle size distribution and mechanical properties of mineral waste slag as filling material. *Constr. Build. Mater.* **253**, 119183 (2020).

22. Tang, X. Y., Wan, W., Zhang, Z. T., Gao, W. H. & Wang, Y. H. Residual deformation of coal gangue subgrade filler under multi-vibration cyclic loading. *Sci. Rep.* **2023**, 13 (2023).
23. Zhang, Z., Gao, W., Liu, C., Liu, Z. & Feng, X. Experimental study on the effect of gradation on the compaction and strength characteristics of coal gangue subgrade filler. *J. Eng. Geol.* **2022**, 89 (2022) ((in Chinese)).
24. Liu, S. *et al.* Study on the influence of coarse aggregate distribution uniformity on the compaction characteristics of gap-graded gravels. *Comput. Geotechn.* **170**, 106293 (2024).
25. Chen, W. B., Yin, J. H., Feng, W. Q., Borana, L. & Chen, R. P. Accumulated permanent axial strain of a subgrade fill under cyclic high-speed railway loading. *Int. J. Geomech.* **2018**, 18 (2018).
26. Cai, Y. Q., Chen, J. Y., Cao, Z. G., Gu, C. & Wang, J. Influence of grain gradation on permanent strain of unbound granular materials under low confining pressure and high-cycle loading. *Int. J. Geomech.* **18**, 04017156 (2018).
27. Leng, W., Xiao, Y., Nie, R.-S., Zhou, W. & Liu, W. Investigating strength and deformation characteristics of heavy-haul railway embankment materials using large-scale undrained cyclic triaxial tests. *Int. J. Geomech.* **17**, 04017074 (2017).
28. Talbot, A. N. & Richart, F. E. The strength of concrete-its relation to the cement, aggregates and water. *Illinois Univ. Eng. Exp. Sta Bull.* **137**, 1–118 (1923).
29. Zhang, Z. & Gao, W. Effect of different test methods on the disintegration behaviour of soft rock and the evolution model of disintegration breakage under cyclic wetting and drying. *Eng. Geol.* **279**, 105888 (2020).
30. Zhang, Z.-T., Gao, W.-H., Zeng, C.-F., Tang, X.-Y. & Wu, J. Evolution of the disintegration breakage of red-bed soft rock using a logistic regression model. *Transport. Geotechn.* **24**, 100382 (2020).
31. Zhang, Z.-T., Gao, W.-H., Wang, X., Zhang, J.-Q. & Tang, X.-Y. Degradation-induced evolution of particle roundness and its effect on the shear behaviour of railway ballast. *Transport. Geotechn.* **24**, 100388 (2020).
32. China, Ministry of transport of the People's Republic of China. *JTG 3430–2020 Test Methods of Soils for Highway Engineering* (China Communications Press, 2020).
33. Garcia-de-la-Oliva, J. L. & Moreno-Robles, J. Granular sub-ballast compaction control methods in high-speed railway lines, Spanish experience. *Transport. Geotechn.* **19**, 135–145 (2019).
34. Trinh, V. N. *et al.* Mechanical characterisation of the fouled ballast in ancient railway track substructure by large-scale triaxial tests. *Soils Found.* **52**, 511–523 (2012).
35. Huang, B., Ding, H. & Chen, Y. Simulation of high-speed train load by dynamic triaxial tests. *Chin. J. Geotech. Eng.* **33**, 195–202 (2011) ((in Chinese)).
36. Huang, J., Ding, Z., Yuan, T., Zhao, D. & Peng, L. Experimental study of dynamic deformation properties of peaty soil under cyclic loading. *Rock Soil Mech.* **38**, 2551–2558 (2017) ((in Chinese)).
37. Zhuang, X., Zhao, H., Wang, J., Huang, Y. & Hu, Z. Quantitative research on morphological characteristics of hysteretic curves of remolded weak expansive soil under cyclic loading. *Rock Soil Mech.* **41**, 1–10 (2020) ((in Chinese)).
38. Cai, Y., Zhao, L., Cao, Z. & Gu, C. Experimental study on dynamic characteristics of unbound granular materials under cyclic loading with different frequencies. *Chin. J. Rock Mech. Eng.* **36**, 1238–1246 (2017) ((in Chinese)).
39. Indraratna, B., Lackenby, J. & Christie, D. Effect of confining pressure on the degradation of ballast under cyclic loading. *Geotechnique* **55**, 325–328 (2005).
40. Xie, D. *Soil Dynamic* (Higher Education Press, 2011).

Acknowledgements

This work was supported by the National Natural Science Foundation of China (52208341), the Natural Science Foundation of Hunan Province (2023JJ40293), Xiaohe Sci-Tech Talents Special Funding under Hunan Provincial Sci-Tech Talents Sponsorship Program (2023TJ-X74), the Scientific Research Projects of Hunan Provincial Department of Education (Grant No. 23B0492). This support is gratefully acknowledged.

Author contributions

L.Z.Z. wrote the main manuscript text; and C.B.K. analyzed the test data; and Z.T.Z. provided the test scheme and revised manuscript.

Competing interests

The authors declare no competing interests.

Additional information

Correspondence and requests for materials should be addressed to Z.-T.Z.

Reprints and permissions information is available at www.nature.com/reprints.

Publisher's note Springer Nature remains neutral with regard to jurisdictional claims in published maps and institutional affiliations.



Open Access This article is licensed under a Creative Commons Attribution 4.0 International License, which permits use, sharing, adaptation, distribution and reproduction in any medium or format, as long as you give appropriate credit to the original author(s) and the source, provide a link to the Creative Commons licence, and indicate if changes were made. The images or other third party material in this article are included in the article's Creative Commons licence, unless indicated otherwise in a credit line to the material. If material is not included in the article's Creative Commons licence and your intended use is not permitted by statutory regulation or exceeds the permitted use, you will need to obtain permission directly from the copyright holder. To view a copy of this licence, visit <http://creativecommons.org/licenses/by/4.0/>.

© The Author(s) 2024